Physica Medica 61 (2019) 33–43

Contents lists available at ScienceDirect

Physica Medica

journal homepage: www.elsevier.com/locate/ejmp

Original paper

Monte Carlo assessment of beam deflection and depth dose equivalent variation of a carbon-ion beam in a perpendicular magnetic field

Mahmoudreza Akbari[a], Alireza Karimian[b,*]

[a] Department of Nuclear Engineering, Faculty of Advanced Sciences and Technologies, University of Isfahan, Isfahan, Iran
[b] Department of Biomedical Engineering, Faculty of Engineering, University of Isfahan, Isfahan, Iran

ARTICLE INFO

Keywords:
MRI-guided carbon-ion radiotherapy
Depth dose equivalent perturbation
Beam deflection
Multi-layer tissue phantom

ABSTRACT

Purpose: To evaluate beam deflection and dose equivalent perturbation of carbon-ion (C-ion) versus depth in a perpendicular magnetic field with the motivation of application to potential future development of MRI-guided carbon therapy.

Methods: A therapeutic beamline, a rectangular water phantom (homogeneous) and a multi-layer tissue phantom were simulated by applying the FLUKA Monte Carlo simulation code. The C-ion beam deflection variation against depth inside the water phantom at 100, 220 and 310 MeV/nucleon (MeV/n) was calculated in the presence of 0.5, 1.5 and 3 T magnetic fields. The 220 MeV/n primary ion depth dose equivalent variations induced by a 1.5 T field were calculated inside the homogeneous and multi-layer phantoms.

Results: The calculated deflections were ranging from 0 to 10.5 mm. The Bragg depth did not change by applying a 1.5 T field to both phantoms under study at 220 MeV/n energy. The dose equivalent in the Bragg depth inside the homogeneous and multi-layer tissue phantoms was found to be reduced by 5.1% and 2.95%, respectively. A dose equivalent reduction of 5.77% in the Bragg depth was obtained when an air layer of 1.8 cm thick was added to the multi-layer phantom.

Conclusion: Dose equivalent perturbation and beam deflection become important at energies above 100 MeV/n, in both phantoms affected by a 1.5 T magnetic field.

1. Introduction

Importance of magnetic resonance imaging (MRI) in radiation therapy (RT) is on a rapid advance. When compared with present and prevalent X-ray based image-guided radiotherapy (IGRT), the MRI reveals greater soft-tissue contrast without supplementary dose to the patient. Consecutive imaging through MR is expected to obtain high accuracy therapies, simplify adaptive radiotherapy techniques, and to track the tumor movement [1–4].

For a more accurate delivery of photon beam therapy, studies have been running on the integration of an MRI and treatment system [3–5], and the clinical feasibility of the MRI-Linac was previously demonstrated [4,6,7].

Integration of MRI field with RT leads to multiple challenges in the treatment process; consequently, MR-guided radiotherapy (MRgRT) has become an important research subject which motivates charged particle beam therapy as well [8,9].

Because for the charged particles both the primary ions and the secondary electrons become affected, the influence of the magnetic field on charged particle beams is more evident than on X-rays [10,11]. Therefore, the contribution of the primary ions and the secondary electrons in the disturbances created by applying the magnetic field should be assessed.

Due to the conceivable advantage of MR-guided proton therapy (MRgPT) over conventional proton therapy, many simulation-based studies have been run. Basic beam transport and dosimetric calculations, particularly the deflection of proton beams by intense uniform magnetic fields, were performed [10,12]. The patient-based treatment planning optimization in uniform magnetic fields has also been of concern [13,14]. The experimental verification for MR-integrated proton therapy has recently run by Schellhammer et al. [15], where the effect of a magnetic field on beam deflection and Bragg peak displacement in a homogeneous phantom material was measured. Meanwhile, Monte Carlo simulations were performed for calculating beam deflection and Bragg peak displacement in the same configuration to the experimental set-up. It was revealed that Monte Carlo simulations could be applied as a gold standard method in predicting the proton beam trajectory in MRgPT [15].

* Corresponding author.
E-mail address: karimian@eng.ui.ac.ir (A. Karimian).

https://doi.org/10.1016/j.ejmp.2019.04.016
Received 5 August 2018; Received in revised form 13 April 2019; Accepted 19 April 2019
Available online 25 April 2019

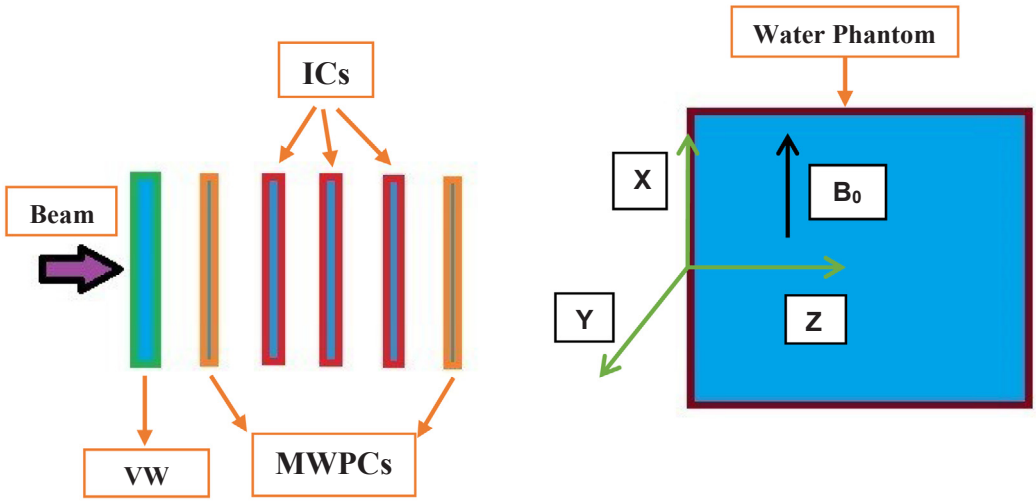

Fig. 1. The schematic of the water equivalent geometry of the HIT beamline (left), the homogeneous water phantom (right) subject to a uniform magnetic field (B_0). One VW, three ICs, and two MWPCs constitute the components of the beam application and monitoring system (BAMS). The X, Y, and Z are the coordinate axes, indicating the applied field direction, beam deflection, and beam axis, respectively. It should be noted that these dimensions are not to scale.

Due to biological and physical advantages (i.e., larger relative biological effectiveness (RBE) and smaller Bragg peak width) [16], the importance of dose transfer accuracy is expected to be more important for carbon than the proton. Hence, C-ion radiotherapy is anticipated to derive a benefit from MRI-guided particle therapy.

However, to the best of the authors' knowledge, there exists no study on transportation of therapeutic C-ion beams in a multi-layer tissue phantom affected by magnetic fields, but Monte Carlo code Gate/Geant4 was applied in calculating the Bragg peak displacement of monoenergetic C-ion beams inside a homogeneous phantom affected by uniform magnetic fields [11]. Due to anatomical changes of tissues and continuous C-ion energy loss in carbon therapy, assessing beam deflection and dose equivalent perturbation of C-ion versus depth in MRI-guided carbon therapy (MRgCT) is a challenge if future potential technological developments are sought.

This assessment was run in this study, where transportation of more realistic C-ion beams inside a tissue slab phantom (as a simplified geometry for a lung tumor patient) was simulated. Although Geant4 is able to transport of C-ions, and can track them in the presence of a magnetic field [11], a slightly less confined dose prediction was reported for simulation of a clinical set-up where the Geant4 toolkit was applied [17]. In comparison with Geant4, it has been revealed that FLUKA Monte Carlo radiation transport code was in good agreement with the experimental data, where it was applied in calculating carbon depth-dose, profile, and nuclear fragmentation products [18–20]. The FLUKA code has a particular option, the *HADROTHErapy*, for applying appropriate physics settings for hadron transport. Moreover, it has a precise and quick algorithm for transporting ions in a magnetic field [21,22].

In this research work, a therapeutic water equivalent beamline for C-ion [18] was simulated through the FLUKA Monte Carlo radiation transport code. Variation of the primary ion deflection against depth was calculated in the presence of uniform magnetic fields inside a water phantom. To the best of the authors' knowledge, for the first time:

I. To evaluate secondary and primary particle contribution in dose perturbation, the deflections of the fluence and total dose profiles in the Bragg peak depth inside a homogeneous phantom were compared;
II. The therapeutic C-ion depth dose equivalent variations generated in the homogeneous and the non-homogeneous phantom affected by the magnetic field were calculated in comparison with the non-field condition;
III. The lateral dose equivalent profile deflection was calculated in the studied phantoms at 220 MeV/n energy and a 1.5 T magnetic field;
IV. After adding a layer of air to the simulated multi-layer tissue phantom, the 1.5 T magnetic field effect, with different step size settings inside the materials, on depth dose equivalent and the lateral dose equivalent profile was assessed.

2. Materials and methods

2.1. FLUKA Monte Carlo code

FLUKA is a multipurpose code capable of transporting charged and non-charged particles in various materials in the presence of magnetic fields. It provides complex particle/boundary interactions and supports the curved path [21,22]. In this study, the FLUKA Monte Carlo code (version 2011.2c.5) was applied to simulate the therapeutic C-ion beam deflection and dose equivalent distortion in phantom materials affected by uniform magnetic fields.

2.2. Materials and geometries applied for the beamline and the water phantom simulation

To yield good agreement with experimental data, water equivalent constituents of the Heidelberg Ion Therapy Center (HIT) beamline, introduced by Parodi et al. [18], was simulated in this study.

The components of the beamline monitor system consist of vacuum window (VW), ionization chambers (ICs), multi-wire proportional chambers (MWPCs), mostly made of low atomic number materials. The VW, the three ICs and the two MWPCs were placed at 1 cm intervals, and simulated as thin layers of 360, 230 and 160 μm water, respectively (see Fig. 1). Because C-ions are heavier in comparison to particles like protons, they are less sensitive to Coulombic collision; therefore, this simplification in the geometry of the beamline is acceptable [18].

To reduce the time/history in the simulation process, the simulated water phantom (as a homogeneous phantom) dimensions were suited for the studied energies. Phantom dimensions of $10 \times 10 \times 10$, $20 \times 20 \times 20$, and $30 \times 30 \times 30\ cm^3$ were chosen for 100, 220 and 310 MeV/nucleon (MeV/n) beam energies, respectively. A uniform magnetic field (B_0) was applied along the +X direction of the coordinate axis inside the water phantom.

According to Parodi et al. [18], 77.3 and 85.7 eV values were selected for water and air ionization potentials from the code's default in all simulations, respectively. Air and water densities assumed to be

Table 1
The simulated primary beams (along the +Z direction) specifications before reaching beam application and monitoring system (BAMS). P is the beam momentum. X and Y are the coordinates perpendicular to the beam direction.

Momentum broadening type (ΔP)	ΔP/P	Beam divergence type	Divergence (Δφ)	Beam spatial distribution along X and Y orientations	FWHM[b] of the fluence profile along X and Y directions (cm)
Gaussian	0.001	Gaussian	1 mrad[a]	Gaussian	0.123 (100 MeV/n) 0.113 (120 MeV/n) 0.078 (220 MeV/n) 0.071 (250 MeV/n) 0.059 (310 MeV/n)

[a] 0.001 rad.
[b] Full width at half maximum.

0.001 and 1 g/cm^3 extracted from the FLAIR material data library, respectively.

2.3. Primary C-ion beam simulation

The simulated primary C-ion beam features, before reaching the water equivalent thicknesses of the monitoring detectors, are shown in Table 1. Therapeutic energies of 100, 120, 220, 250, and 310 MeV/n were assessed. Energies of 120 and 250 MeV/n were assessed only to verify the reproducibility of data reported by Fuchs et al. [11], who calculated the Bragg peak deflection at the above-mentioned energies. The spatial distribution data of the primary beam was extracted from the HIT beam library, and their change follows a logarithmic pattern. The energy broadening mean values together with the spatial angular distribution was extracted from common values available in C-ion foci libraries [18].

2.4. Simulation validation in the homogeneous phantom

For this purpose, the relative depth dose curves of C-ion beams were compared with the available experimental data [23]. Not all of the studied energies were validated because we did not have access to the experimental dose profile data at these energies. Validation was performed only for depth dose profiles at 100, 220, and 310 MeV/n energies.

2.5. Depth dose equivalent distribution and the primary beam deflection in the homogeneous environment

Variations in primary ion depth dose equivalent due to the presence of a 1.5 T magnetic field were calculated and compared with the non-field condition at 220 MeV/n beam energy.

To calculate the deflection of the primary C-ions at different depths inside the water phantom, the shifted values of the primary particle fluence profiles centers (compared to non-field condition) were obtained in the presence of the studied magnetic fields.

FWHM of the fluence profiles was obtained by calculating the fluence profile width in half of its maximum value and were compared at a specific depth between the cases of the magnetic fields' presence or absence.

The deflections of the relative fluence and total dose profiles in the Bragg peak depth of 220 MeV/n energy, in the presence of a 1.5 T magnetic field (average therapeutic energy and median diagnostic field), were compared to assess the primary and secondary particles contribution in dose distortions-induced by the magnetic fields.

2.6. Simulated multi-layer tissue phantom

To model a patient with lung tumor in a simplified geometry, a rectangular multi-layer tissue phantom (Fig. 2) with 10 × 10 × 12.2 cm^3 dimensions containing (0.2 cm) skin, (1 cm) fat tissue, (3 cm) striated muscle, (1 cm) compact bone, two (2 cm) lung soft tissue layers containing blood, (3 cm) tumor with material densities of: 1.1 (skin), 0.92 (fat), 1.04 (muscle), 1.85 (bone), 1 (lung tumor), 1.05 (local density of the lung) in g/cm^3, was simulated. The tissues' compound and their densities were extracted from the FLAIR (FLuka Advanced InteRface) material data library. Ionization potential values of the simulated tissues were set to the code defaults. The simulated initial C-ion depth dose equivalent was compared between the presence and absence of a 1.5 T magnetic field at 220 MeV/n ion beam energy. FWHM of the Bragg peak was compared as to the presence and absence of a 1.5 T magnetic field.

The deflection of dose equivalent profile in the Bragg depth, defined as the profile center displacement value obtained by applying the magnetic field compared to the case without the magnetic field, was calculated at 220 MeV/n beam energy subject to a 1.5 T magnetic field (B_0).

To be comparative with the calculations ran on protons in the inhomogeneous media [10], 1.5 T field impact inside the simulated heterogeneous phantom was assessed, first, by adding an air layer of 1.8 cm thickness just before the depth equals to the Bragg depth inside the multi-layer phantom without the air layer (at a depth of 7.2–9 cm), next, the depth dose equivalent and dose equivalent profile curves were compared between the presence and absence of a 1.5 T field. Under this circumstance, the tumor layer thickness became 1.2 cm.

A USRBIN detector together with the AUXSCORE card was applied in calculating the primary ion fluence profiles, depth dose equivalent, total dose profile and lateral dose equivalent profile distributions. In the FLUKA code, the particles' dose equivalent for which conversion coefficients are not accessible, usually heavy ions, can be computed by scoring the generalized particle DOSEQLET. Dose equivalent is calculated through the Q (LET) equation as specified in ICRP publication [24], where LET is unrestricted linear energy transfer (LET_∞) in water [21]. The quantity dose equivalent, H, is expressed as:

$$H = Q \times \mathrm{D} \tag{1}$$

where Q is the quality factor and D is the absorbed dose at the point of concern. Here, the value of Q is determined by the charged particles' type and energy crossing a small volume element at this point. The quality factor Q at a point in the tissue is expressed as:

$$Q = \frac{1}{D}\int_{L=0}^{\infty} Q(L) D_L dL \tag{2}$$

where D (L) is the distribution of D in L for the charged particles contributing absorbed dose at the point of concern. L is the unrestricted LET. Q (L) is calculated as follows [24]:

$$Q(L) = \begin{cases} 1 & \text{for} \quad L<10\,\mathrm{keV/\mu m} \\ 0.32\,L - 2.2 & \text{for} \quad 10 \le L \le 10\,\mathrm{keV/\mu m} \\ 300/\sqrt{L} & \text{for} \quad L>10\,\mathrm{keV/\mu m} \end{cases} \tag{3}$$

Bin size in depth was selected within 0.2 mm up to 2 mm depending on energy and location on the Bragg curve (as the depth increased and approached the Bragg region, the smaller bin size was selected). For depth dose equivalent calculation, a cylindrical mesh with 10 mm

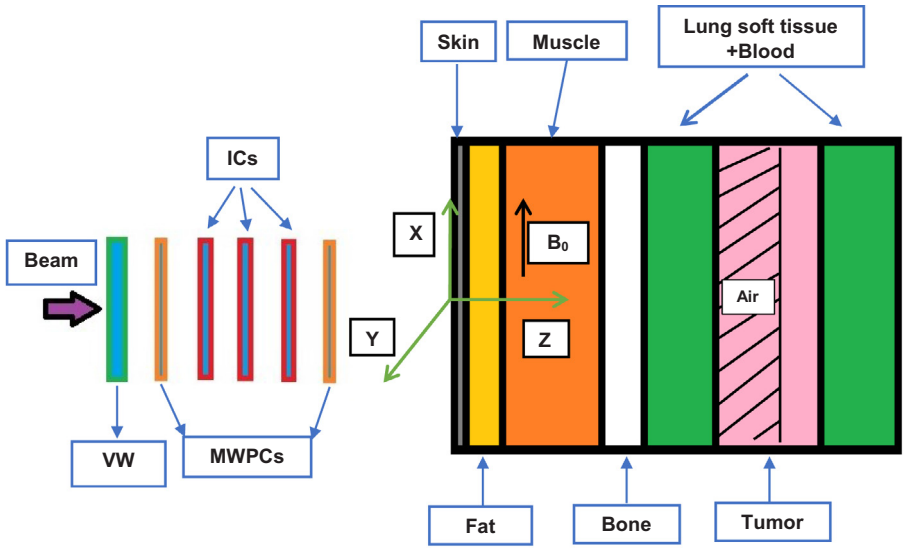

Fig. 2. Schematic diagram of the water equivalent geometry of the HIT beamline (left) and multi-layer tissue-like heterogeneous phantom (right) influenced by a 1.5 T field (B_0). The tissue layers from left to right: (0.2 cm) skin, (1 cm) fat, (3 cm) striated muscle, (1 cm) compact bone, and two (2 cm) lung soft tissue layers containing blood sandwich (3 cm) tumor, respectively. The axes X, Y, and Z are the coordinate axes, indicating the direction of the applied field, beam deflection, and beam axis, respectively. The air layer that replaces the lung tumor layer is shown in the humped area. In this schematic, dimensions are not to scale.

diameter and 0.2–2 mm height was applied. In this simulation, for the one-dimensional total dose, dose equivalent and fluence profiles along the transverse direction, a rectangular mesh with dimensions of $1 \times 0.5 \times 0.5\,mm^3$ was applied.

The maximum number of 1.7×10^7 initial C-ions histories was tracked to reach statistical accuracy less than 1% at the fluence, total dose, and dose equivalent calculations. The MGNfield card involved in applying 0.5, 1.5 and 3 T magnetic fields along the +X direction inside the simulated phantoms. The minimum and maximum step sizes were set through STEPSIZE card inside the tissue layers for charged particle transportation. The maximum step size for a given region can be decided based on the following considerations:

I. In a region with the magnetic field, the step size should not exceed its neighboring regions and the minimum dimensions.
II. It is chosen larger than the minimum step forced by MGNFIELD or by STEPSIZE itself.
III. To allow the multiple scattering algorithm to be run in its optional sense, in all non-vacuum simulated regions, this size is not chosen smaller than one-third of its minimum dimension.

STEPSIZE card sets the minimum and the maximum step sizes on a region-by-region basis for transport of all charged particles. It should be noted that the MGNFIELD card has an important option for setting the step size in case of tracking in a magnetic field. In case of conflict with STEPSIZE, STEPSIZE card overrides region by region the overall minimum step set by the MGNFIELD card (if larger than it). To help the code to attain the required tracking accuracy in a magnetic field, the other parameters that are recommended to be reasonably set by MGNFIELD and STEPSIZE cards are the maximum angle in a sub-step and the maximum error in the boundary identification [21].

Based on above-mentioned recommendations [21] as well as considering the minimum and maximum dimensions in the simulated phantoms, the minimum step size was set to 0.05 cm in the MGNFIELD card. In STEPSIZE card, the minimum step size was set to 0.05 cm, and the maximum was set ranging 0.08–2 cm in the case of multilayer heterogeneous phantom. The maximum angle in a sub-step and the maximum error in the boundary identification were set to 30 degrees and 0.03 cm, respectively.

The effect of step size value changes in the predicted variations through the simulation code was assessed in the presence of the air layer in the phantom. The step size was set to 0.05 cm in the MGNFIELD card. The minimum step sizes of 0.1, 1 and 2 cm were adjusted through the FLUKA STEPSIZE card. The maximum step size was fixed to 3 cm in this case. The maximum angle in a sub-step and the maximum error in the boundary identification were set to 30 degrees and 0.03 cm, respectively. The depth dose equivalent and lateral dose equivalent profile curves subject to the above conditions were compared, where the other simulation parameters were assumed constant.

Outside the simulated homogeneous (with dimensions of $10 \times 10 \times 10$ up to $30 \times 30 \times 30\,cm^3$) as well as heterogeneous phantoms, the magnetic field intensity was considered to be zero. For all simulations applied in this research, *HADROTHErapy* option, which sets appropriate physics to hadron transport, was activated in the DEFAULT card of the code.

3. Results

3.1. Beamline simulation validation

To validate the C-ion beamline simulation, the simulated relative depth dose curves at 100, 220, and 310 MeV/n energies are compared to the available experimental data, relevant to the most similar beamline components to the one simulated, in the published literature [23], Fig. 3. It is revealed that there exists good agreement (from 1.5 ± 0.2 up to 2.5 ± 0.2 mm accuracy) regarding the Bragg peak depth prediction, between the finding here and that of experimental data [23], in the absence of the magnetic field.

3.2. Transport within the water phantom affected by the uniform magnetic fields

3.2.1. Depth dose equivalent perturbation and the primary beam deflection

The simulated depth dose equivalent distribution of a 220 MeV/n carbon beam in the homogeneous water phantom is compared between 0 and 1.5 T magnetic fields in Fig. 4. Because the change in depth dose equivalent curve in the plateau area (flat area in the carbon depth dose) is negligible when a 1.5 T field is applied, the curves are compared only from a depth of 8 cm (after the plateau ends), where as observed, the maximum depth dose equivalent does not change (with 0.2 mm uncertainty). The dose equivalent in the Bragg depth reduces by 5.1% due to applying a 1.5 T field in comparison to the non-field condition. To better display the graphs, a great number of data points are omitted from the curves.

Because the variation of the dose equivalent, due to applying the field, is not easily recognizable in Fig. 4, the percentage of the dose equivalent change after adding a 1.5 T magnetic field is plotted against depth in Fig. 5. The vertical axis value is calculated through Eq. (4):

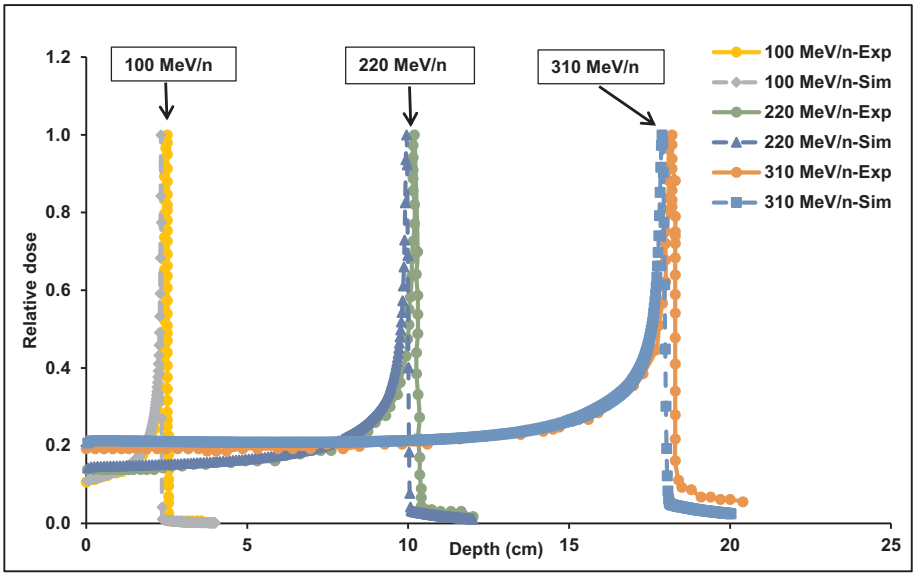

Fig. 3. The simulated relative depth dose curves in the water phantom, in the absence of the magnetic fields at 100, 220 and 310 MeV/n C-ion beam energies compared with that of the experimental data (dashed line: this study and solid line: extracted from Ref. [23]).

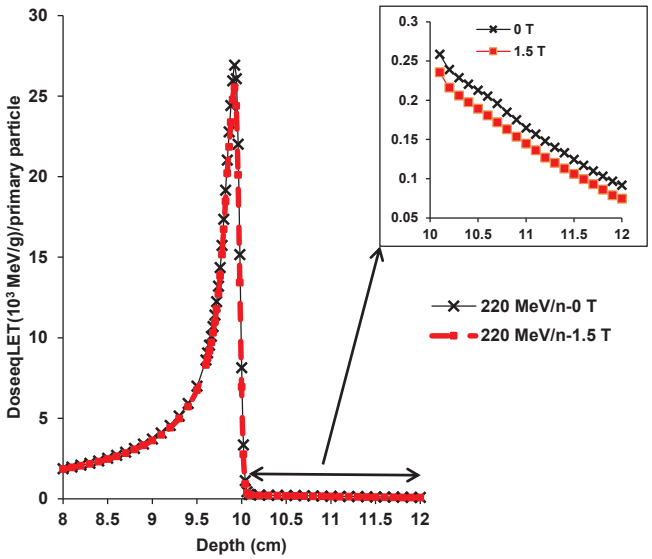

Fig. 4. Comparison of the primary particle depth dose equivalent curves in the homogeneous water phantom. The studied energy is 220 MeV/n in the presence of 0 (solid line) and 1.5 T (dashed line) magnetic fields. On the vertical axis, "DoseeqLET" is dose equivalent, which is a score option in the FLUKA code. A smaller graph, in the upper right corner of the main chart, is plotted to better display the effect of the magnetic field on the tail area of the curve.

$$\text{Percentage of decrease in dose equivalent (\%)} = \frac{(\text{DeqLET})1.5\text{ T} - (\text{DeqLET})0\text{ T}}{(\text{DeqLET})0\text{ T}} \times (-100) \quad (4)$$

where in this equation, (DeqLET)0 T and (DeqLET)1.5 Tare the dose equivalent in the presence of 0 and 1.5 T fields, respectively.

Maximum change in dose equivalent is 18.5%, which occurs at the curve tail (at 11.88 cm depth).

The alteration of the fluence profile lateral shift (beam deflection) at different depths is shown in Fig. 6. The assessed energies are 100, 220 and 310 MeV/n in the presence of 0.5, 1.5, and 3 T magnetic fields. Because the deflection value of 100 MeV/n energy is zero at 0.5 and 1.5 T magnetic fields, they are not shown in Fig. 6. For particular energy, an increase in depth increases the lateral shift of the fluence

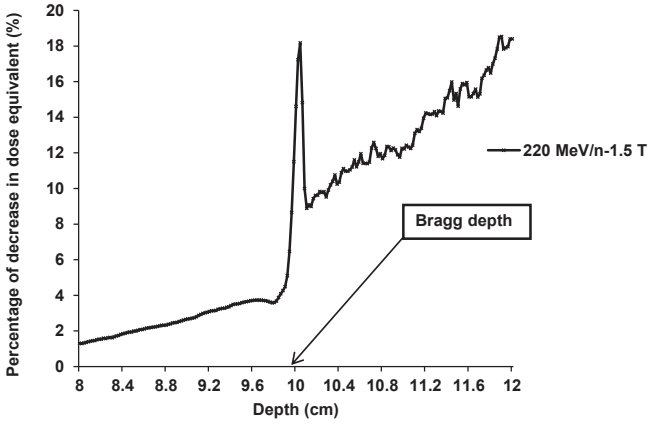

Fig. 5. Percentage of decrease in C-ion dose equivalent against depth at 220 MeV/n beam energy after applying a 1.5 T field to the homogeneous phantom.

profile.

To reproduce the data reported in lateral dose profile deflection form [11], the dose equivalent profile deflection in the same energies (i.e., 120 and 250 MeV/n) and the similar magnetic field intensity (i.e., 3 T) was assessed, which found to be 0.50 ± 0.25 mm and 5.75 ± 0.25 mm, respectively.

A 220 MeV/n C-ion fluence profile (including primary, secondary, and tertiary) at different depths of the homogeneous phantom in the presence of a 1.5 T field is diagrammed in Fig. 7.

The FWHM of the fluence profile does not change at a particular depth by applying the magnetic field. The profile center displacement is within 0–10.5 mm with 0.5 mm uncertainty (within 0–3 T magnetic field strength and 100–310 MeV/n energy range).

To better display distortion variations due to depth change, the deflection changes of the fluence profile centers against the water phantom depth, at 220 MeV/n energy in the presence of the magnetic fields studied, are shown in Fig. 8. Although this selection is almost arbitrary, thus, a fourth-degree polynomial curve is considered as an appropriate fit, while there exists the possibility that a third-degree polynomial curve would serve the purpose as well. In all curve fittings, R^2 values are better than 0.99.

The deflection of the fluence and total dose profiles at 220 MeV/n

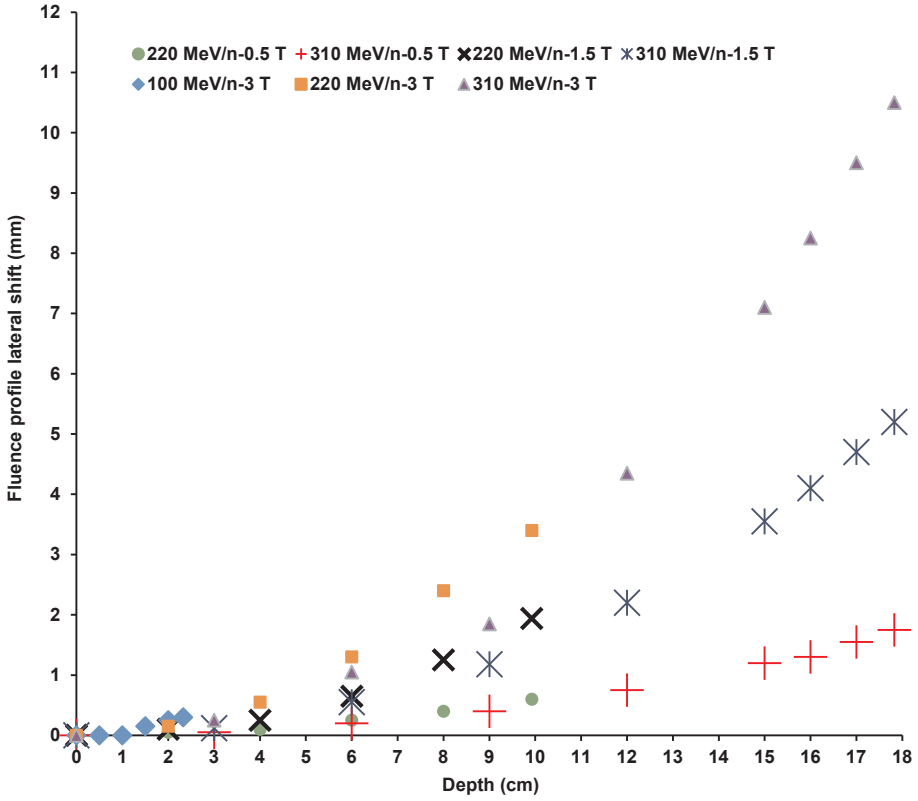

Fig. 6. Changes in the fluence profile deflection (beam deflection) against phantom depth. The assessed energies are 100, 220 and 310 MeV/n, where the magnetic fields with 0.5, 1.5 and 3 T strength are affected on the homogeneous phantom.

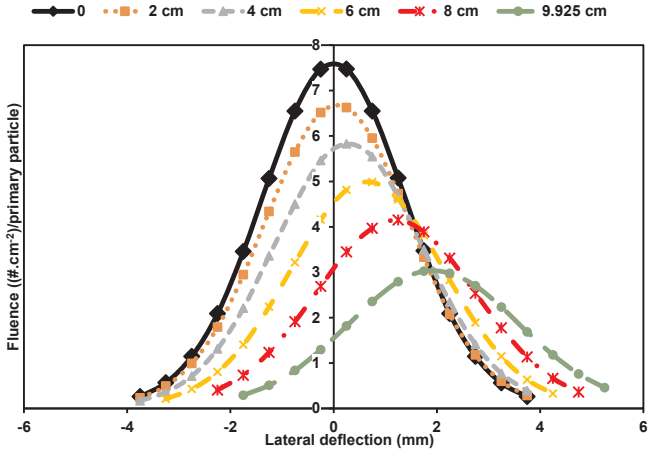

Fig. 7. A 220 MeV/n C-ion total fluence profiles (per primary particle) at different depths (up to the Bragg depth at 9.925 cm) in the presence of a 1.5 T magnetic field (due to high statistical relative errors, some data points, especially at further distances from the beam center, in the transverse direction, are omitted).

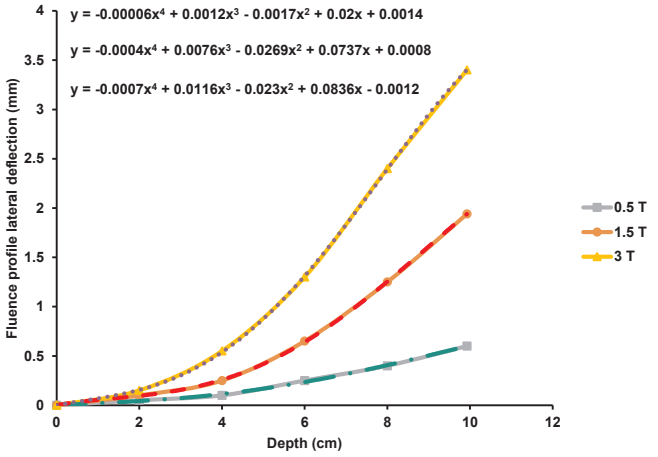

Fig. 8. Variations of the deflection of the fluence profiles centers against the homogeneous phantom depth at 220 MeV/n energy in the presence of 0.5, 1.5, and 3 T magnetic fields. From top to bottom, the fitted curves' (dashed lines on the main curves) equations relate to 0.5, 1.5 and 3 T fields, respectively.

energy in the presence of a 1.5 T magnetic field are more or less the same at different depths before reaching the Bragg peak, while it is revealed that this value is slightly greater (less than 0.30 ± 0.25 mm) for the fluence profile at the Bragg peak depth (see Fig. 9).

3.3. Effect of the magnetic field on the depth dose equivalent and lateral dose equivalent profile distributions in the multi-layer tissue phantom

The depth dose equivalent distribution of a 220 MeV/n C-ion beam in the presence and absence of a 1.5 T magnetic field inside the tissue slab phantom is shown in Fig. 10. As can be seen, the depth of the maximum dose equivalent does not change (with 0.5 mm uncertainty) by the influence of the magnetic field. By applying the magnetic field, the dose equivalent is reduced by 2.95% at the Bragg depth in comparison with the non-field condition. The FWHM of the Bragg peak does not change (with 0.2 mm uncertainty) when a magnetic field is applied to the phantom. To better represent the graphs, a great number of data points are removed from the curves.

Because the changes of the dose equivalent by the impact of the field are not easily differentiable in Fig. 10, the percentage of the dose equivalent variation due to applying a 1.5 T magnetic field is shown against depth in Fig. 11.

The maximum variation in the dose equivalent is 18.6% (in

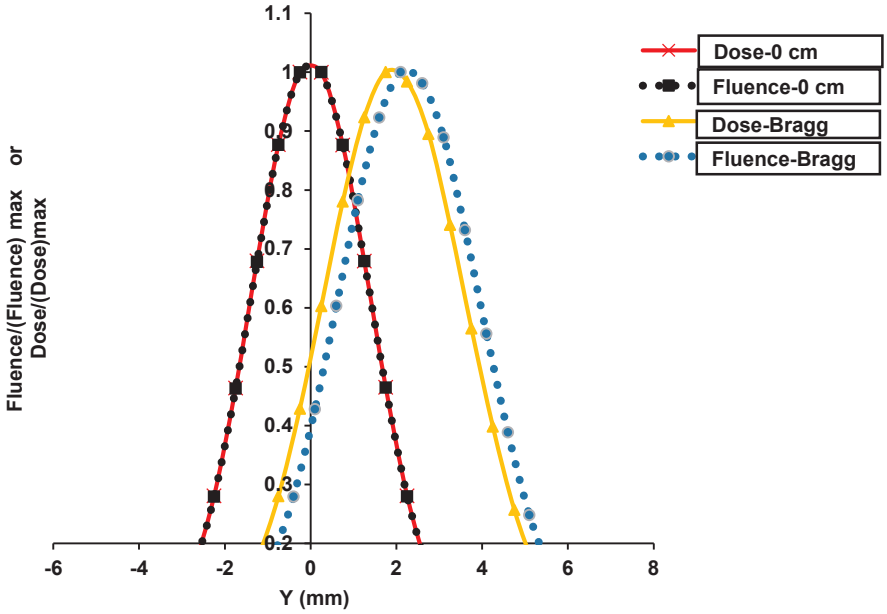

Fig. 9. Comparison of the relative fluence and total dose profiles (per primary particle) at 0 cm and the Bragg depths at 220 MeV/n C-ion energy in the presence of a 1.5 T magnetic field (due to high statistical relative error, some data points are omitted).

comparison to 18.5% for the homogeneous phantom) and occurs at the Bragg curve tail (at 12.07 cm depth).

The lateral dose equivalent profile deflection of a 220 MeV/n carbon beam in the Bragg depth inside the multi-layer tissue phantom, in the presence of a 1.5 T field, was calculated. The dose equivalent profile lateral shift in the heterogeneous tissue phantom is 1.70 ± 0.25 mm compared to 1.96 ± 0.25 mm inside the homogeneous water phantom.

The variation of the depth dose equivalent in the inhomogeneous phantom containing 1.8 cm thick air layer is compared between the presence and absence of a 1.5 T magnetic field in Fig. 12. Meanwhile, the effect of the selected step sizes of 0.1, 1 and 2 cm for charged particle transport is shown in this figure.

As expected, this added air layer increases the Bragg depth in its thickness equivalent. The selected step sizes, for transporting the particles in the presence of a 1.5 T magnetic field, do not change the Bragg depth. Because the changes in dose equivalent are not detected easily in Fig. 12, the depth dose equivalent variation due to a 1.5 T field with 0.1, 1 and 2 cm step sizes settings, is expressed as a percentage of reduction in dose equivalent in a separate diagram (see Fig. 13).

This reduction, calculated through Eq. (4), at the Bragg depth due to

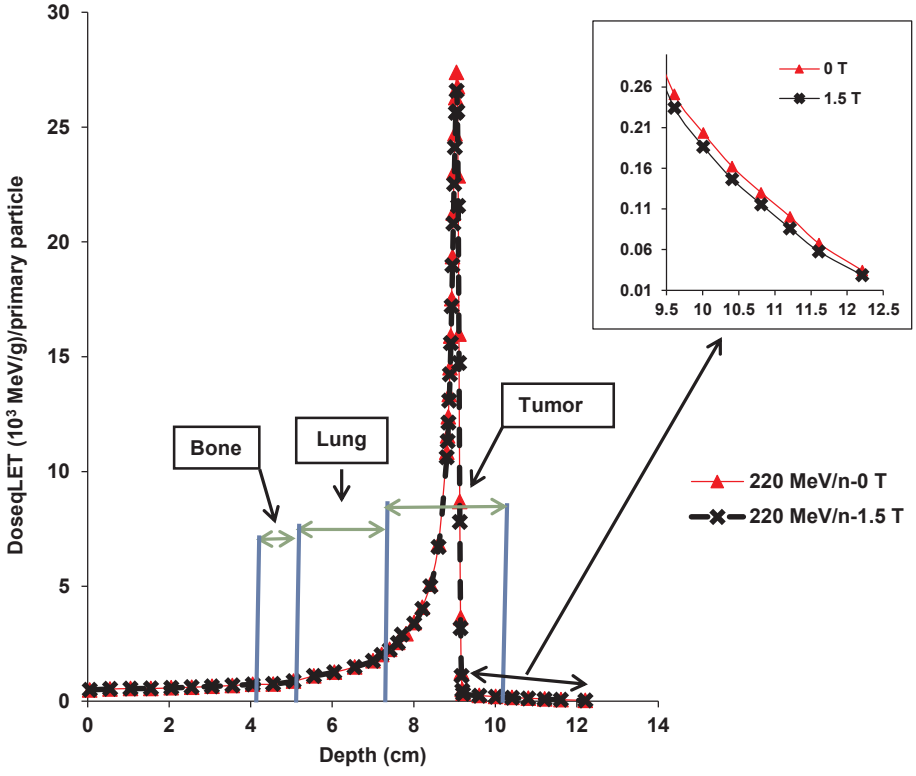

Fig. 10. Comparison of the depth dose equivalent distribution of a 220 MeV/n carbon beam between the presence and absence of a 1.5 T magnetic field within the tissue slab phantom. A smaller chart, in the upper right corner of the main chart, is plotted to better represent the effect of the magnetic field in the tail region of the curve.

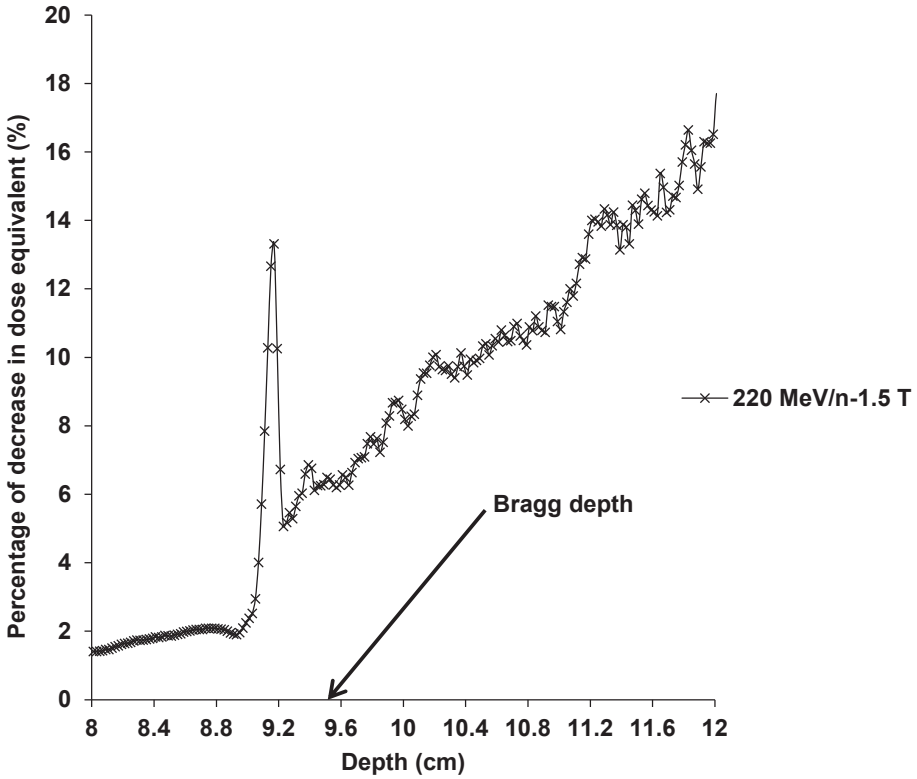

Fig. 11. Percentage of decrease in dose equivalent against depth at 220 MeV/n beam energy due to applying a 1.5 T field to the tissue-like slab phantom.

applying a 1.5 T field is 5.77, 5.92, and 5.71 percent at 0.1, 1 and 2 cm step sizes, respectively. The maximum reduction in dose equivalent for 0.1, 1, and 2 cm step sizes consist of −30.87, −29.67, −30.29%, which occurs at 10.92 cm depth (0.8 mm after the Bragg depth), respectively.

In addition to abrupt changes made in the Bragg depth, observable changes occur at the lung-air and tumor-air boundaries, which in a certain degree depend on the selected step size.

As to the uncertainty range in the calculations run in this study, the deviation magnitude of the dose equivalent profile at the Bragg depth in the heterogeneous phantom with air layer, by applying a 1.5 T magnetic field, is 2.25 ± 0.5 mm (compared to 1.70 ± 0.5 mm for the same without air layer).

4. Discussion

FLUKA code allows the application of different physics settings for charged particle transport. A physics setting recommended for hadron

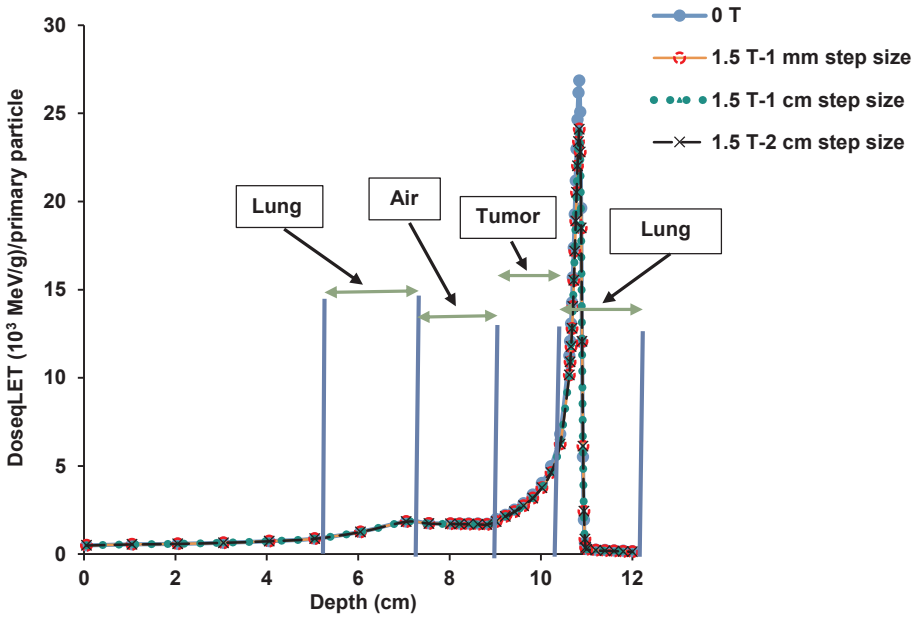

Fig. 12. The effect of a 1.5 T magnetic field on depth dose equivalent in the multi-layer phantom with a 1.8 cm thick air layer at 0.1, 1, and 2 cm minimum step size settings.

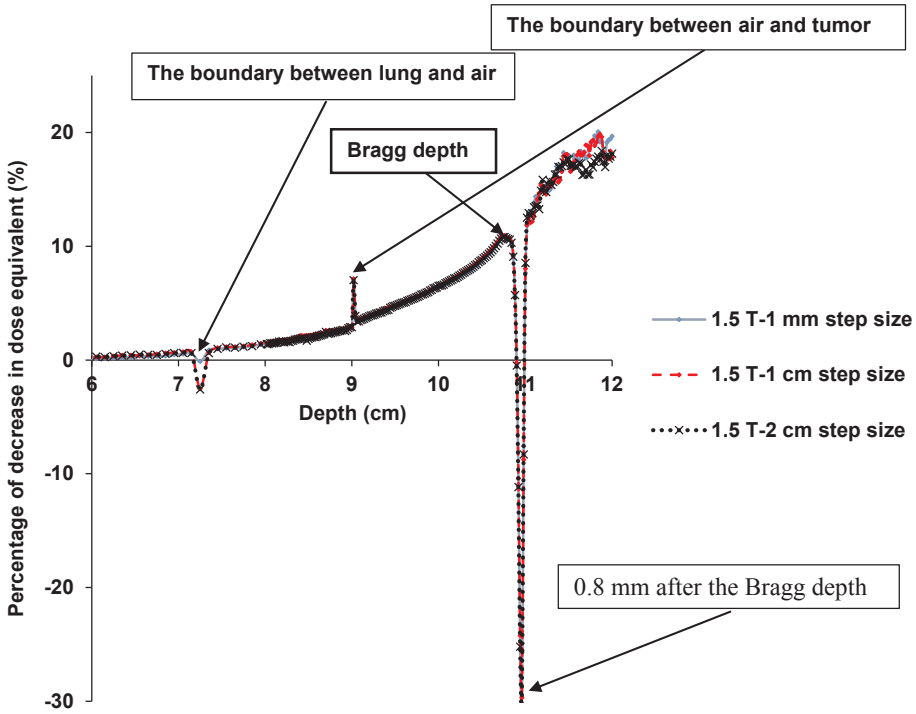

Fig. 13. The reduction percentage in dose equivalent (normalized to the non-field condition) inside a multi-layer phantom containing air layer by adding a 1.5 T magnetic field with 0.1, 1 and 2 cm minimum step sizes selected for charged particle transport.

transport [21] was applied in this study. The validity of the FLUKA application in C-ion beam therapy was already expressed [18,19]. The capability of this code for accurate tracking of charged hadrons was proved, even in cases of more complex magnetic fields [22], while, to the best of the authors' knowledge, no experimental data exists on carbon beams transportation affected by magnetic fields.

The challenges of MRgCT are more than MRgRT because, in addition to the produced secondary particles, the primary particle itself is directly affected by the applied magnetic field. Prediction of disturbances in dose equivalent of the carbon beam generated from applying magnetic fields in the homogeneous and tissue-like slab phantoms will be very contributive in estimating the dose equivalent distribution in the patient's body thus leads to find a solution to compensate for these perturbations.

In this study, for the first time, the deflection of the fluence and total dose profiles in the Bragg peak depth, inside the homogeneous phantom, at average therapeutic energy and median diagnostic field, was assessed to evaluate secondary and primary particle contribution in dose distortion. The dose equivalent disturbances in the homogeneous water phantom and the tissue slab phantom (as a simplified model of the chest geometry of a patient with lung cancer) were assessed through the Monte Carlo method as well.

Regarding the validation of the simulated beamline (see Fig. 3), because of the technical limitations, the minimum thickness of the sensitive volume of the detector, perpendicular to the beam axis, was typically in the range of mm in experimental studies [18,23]. For instance, in the case of researches published by Weber and Kraft [23] and Parodi et al. [18], this thickness was 3 and 2 mm, respectively. However, in our simulation scenario, we derived a benefit from the capability of the FLUKA code in dosimetry, by applying the USERBIN card. So, the minimum thickness of the cylindrical bin detectors was considered to be 0.2 mm, which will yield more accurate results in terms of the Bragg peak location detection.

Similar results, which are presented in Fig. 6, were previously reported by Fuchs et al. [11] through Monte Carlo simulations. They calculated the displacement of monoenergetic C-ion dose profile in the Bragg peak depth of 120 (0, 0.2, and 0.7 mm), 250 (0.7, 1.9, and 5.7 mm), and 400 (2.4, 6.9, and 20.7 mm) MeV/n energies in the presence of 0.35, 1, and 3 T magnetic fields inside a homogeneous phantom, respectively. They modeled a simple monoenergetic beam, while here a more realistic beam was simulated. To reproduce the findings obtained by Fuchs et al. [11], the dose equivalent profile deflection was calculated in the same energies (120 and 250 MeV/n) and the similar magnetic field intensity (3 T). The dose equivalent profile deflection was 0.50 ± 0.25 mm and 5.75 ± 0.25 mm for 120 and 250 MeV/n energies, respectively. Therefore, in computational uncertainty range, the maximum difference between the calculated dose equivalent profile deviation obtained here and the dose profile deflection reported by Fuchs et al. [11], is 0.2 mm.

The maximum value of the transverse deflection and longitudinal displacement of the Bragg peak reported in the literature [10,11,13] are 98.9 and 20.5 mm, respectively, relevant to the maximum therapeutic proton energy of (250 MeV) in the presence of 3 T magnetic field [11]. The maximum lateral shift and longitudinal displacement for C-ion at the maximum energy calculated by Fuchs et al. [11], (400 MeV/n energy), in the presence of 3 T magnetic field, are 20.7, and 0.9 mm, respectively.

Because C-ions have greater mass compared to that of particles like protons, their sensitivity to range straggling is much less. Moreover, they have lower charge-to-mass-ratio, leading to a much lower sensitivity to magnetic fields. This behavior leads to a lower overall beam deflection compared to protons; therefore no deformation of the Bragg peak region as to protons is observed [11].

C-ion advantages like the higher relative biological effect (RBE), lower lateral scattering, and more compressed Bragg peak at the beam edge compared to that of the protons [25,26] lead to the high sensitivity of C-ion radiotherapy to the geometrical variations in the patient [27]. The C-ion exclusive ability can target potential radio-resistant tumors near the soft tissue critical structures' vicinity. This indicates that C-ion radiotherapy guidance through MRI could be more beneficial in the above-mentioned cases compared to MRgPT. However, both MRgCT and MRgPT pose challenges which are to be met.

The difference between the deflection of the fluence and the total dose profiles at 220 MeV/n energy and a 1.5 T field applied, is possibly due to the high ionization density in the Bragg peak and the contribution of the secondary electrons in the dose profile center displacement (see Fig. 9). In this figure, the difference between the centers of dose and fluence profiles displacements is within the uncertainty range of the calculations performed (i.e., 0.5 mm) and it can be neglected. Consequently, the fluence profile displacement can be considered as an acceptable estimate of the total dose profile deviation, and thus, without transportation of the secondary particles to calculate the total dose, running time to perform the Monte Carlo calculations can be reduced.

As observed in Figs. 4 and 10, in the depth dose equivalent curves inside the homogeneous and heterogeneous tissue slab phantoms, in the total uncertainty range of calculations (0.5 mm), the Bragg depth does not change when a 1.5 T magnetic field is applied. This phenomenon is in a good agreement with the longitudinal shift of the Bragg peak at 250 MeV/n in the presence of 1 T field (0.2 mm) found by Fuchs et al. [11].

When C-ion therapy is guided by MRI, similar to MRgPT, the generated secondary electrons are less energetic than that of the photon therapy, indicating that the electron return effect (ERE) is not as important as in photon therapy guiding by MRI [10]. However, ERE has a detectable impact on dose equivalent perturbation in tissue-air boundaries in MRgCT.

In the presence of a 1.5 T field applied at 220 MeV/n energy, the dependency of dose equivalent perturbation on the minimum step size changes is assessed for three different steps. Contrary to expectation, in the range of computational uncertainty, a significant change is not observed, especially in the dose equivalent profile deflection in the heterogeneous phantom with the air layer.

However, in heterogeneous phantom without air layer, there is a reduction of the dose along the central axis of the beam, but this does not directly translate into a reduction of the total dose outside the target. There is a lateral shift of the dose.

To the best of the authors' knowledge, no assessment has been performed on the effect of the uniform magnetic field in parallel with the beam direction concerning neither proton nor carbon traversing in either homogeneous or heterogeneous environment. According to Oborn et al. [28], the effect of the magnetic field is more significant when perpendicular to the beam axis. An attempt was made in this study to assess the changes occurring in the worst scenario, which is induced by the transverse magnetic field effect.

A magnetic field prior to the simulated homogeneous and heterogeneous phantoms would lead to defection of the entire beam before reaching the surface of the phantoms, which leads to change the final deflection of the beam in the phantoms. This should be noted because it will certainly be a consideration in future technological development. In this research study, a uniform magnetic field application effect just within the simulated phantoms has been considered.

5. Conclusion

In brief, as a first attempt, the effect of 0.5, 1.5 and 3 T magnetic fields on fluence distributions of therapeutic C-ion beam in a homogeneous water phantom was assessed by applying the Monte Carlo technique. Moreover, the effect of a 1.5 T field on depth dose equivalent perturbation and lateral dose equivalent profile deflection was assessed at 220 MeV/n C-ion energy within the homogeneous and a heterogeneous phantom.

The findings here are expressed as follows:

I. The C-ion beam deflection variation against the homogeneous phantom depth is described by a fourth-degree polynomial curve;
II. The maximum dose equivalent depth, in both the phantoms at 220 MeV/n energy, does not vary by 1.5 T magnetic field impact;
III. The deflection value of the C-ion fluence profile in the water phantom induced by a 1.5 T field is slightly greater than the total dose profile deflection in the Bragg peak depth of 220 MeV/n energy;
IV. In both the phantoms, at 220 MeV/n energy, the dose equivalent in the Bragg depth decreases when a 1.5 T magnetic field is applied;
V. In both the phantoms, the maximum variation in dose equivalent, due to applying a 1.5 T field, occurs at the Bragg curve tail at 220 MeV/n energy;
VI. Dose perturbation is mostly due to the primary beam deflection and generated secondary electrons have a slight contribution in dose distortions-induced by the magnetic field;
VII. Addition of an air layer in the area before the Bragg depth (at 220 MeV/n energy), inside the multi-layer phantom, increases the reduction percentage in the dose equivalent at the Bragg depth by applying a 1.5 T field;
VIII. Dose equivalent reduction (at 220 MeV/n energy) is subjected to particle transport step size in the presence of a 1.5 T magnetic field;
IX. Any change in step size does not affect the prediction of a change in the Bragg peak depth (at 220 MeV/n energy) due to the effect of the applied 1.5 T magnetic field;
X. There is an obvious impact of the step size on the dose at different density interfaces.
XI. At the boundary between tissue and air, due to the application of a 1.5 T field, significant changes occur in dose equivalent (at 220 MeV/n energy), which to some extent depend on the selected step size for the particle transport;
XII. Because applying the Monte Carlo technique is time-consuming in particle transport calculations, in the case of C-ion in specific, which generates many secondary particles and nuclear fragments, the results obtained here indicate that the calculation of the fluence profile deviation of the primary particles would yield an acceptable approximation in calculating the total dose profile deflection without any need to track the secondary particles.

Clearly, there is an impact due to the presence of the air and heterogeneities do impact the dose distribution in C-ion based MRgRT. However, further study is required into the impact of geometric variations on the dose distortions, which can be an interesting topic for future research.

Here it is found that the dose equivalent perturbation and beam deflection of the therapeutic C-ion beam energies above 100 MeV/n induced by a 1.5 T magnetic field inside the simulated phantoms is of significance.

As the last point, researchers must be fully perfect for implementing MRgRT, and the obtained results will be applicable to future research in MRgCT.

Funding sources

This work was supported by the support program of the Ph.D. thesis at the University of Isfahan, Isfahan, Iran.

Acknowledgements

The authors would like to extend their special thanks to FLUKA support team for members for their assistance regarding the FLUKA discussions. Furthermore, the authors express their deepest gratitude to Prof. Katia Parodi from Ludwig Maximilian University of Munich and Dr. Hermann Fuchs from Medical University of Vienna, Dr. Uli Weber from Philipps University of Marburg and Dr. Gerhard Kraft from Martin-Luther University of Halle-Wittenberg for their permission to apply the data found in their articles.

Competing interests

The authors have no competing interests to declare.

References

[1] Lagendijk JJW, Vulpen M, Raaymakers BW. The development of the MRI linac system for online MRI-guided radiotherapy: a clinical update. J Intern Med 2016;280:203–8.
[2] Yun J, Wachowicz K, Mackenzie M, Rathee S, Robinson D, Fallone BG. First demonstration of intrafractional tumor-tracked irradiation using 2D phantom MR images on a prototype linac-MR. Med Phys 2013;40(051718):1–12.
[3] Palacios MA, Bohoudi O, Senan S, Slotman B, Bruynzeel A, Lagerwaard FJ. MR-guided adaptive stereotactic radiotherapy: a new paradigm in radiotherapy. Phys Medica 2017;44:1.
[4] Van der Heide UA. MR-guided radiation therapy. Phys Medica 2016;32:175.
[5] Wooten HO, Green O, Yang M, DeWees T, Kashani R, Olsen J, et al. Quality of intensity modulated radiation therapy treatment plans using a ^{60}Co magnetic resonance image guidance radiation therapy system. Int J Radiat Oncol Biol Phys 2015;92:771–8.
[6] Kolling S, Oborn B, Keall P. Impact of the MLC on the MRI field distortion of a prototype MRI-linac. Med Phys 2013;40(121705):1–10.
[7] Raaymakers BW, Jürgenliemk-Schulz IM, Bol GH, Glitzner M, Kotte ANTJ, van Asselen B. First patients treated with a 1.5 T MRI-Linac: clinical proof of concept of a high-precision, high-field MRI guided radiotherapy treatment. Phys Med Biol 2017;62:41–50.
[8] Kontaxis C, Bol GH, Lagendijk JJW, Raaymakers BW. Towards adaptive IMRT sequencing for the MR-linac. Phys Med Biol 2015;60:2493–509.
[9] Smit K, Sjöholm J, Kok JGM, Lagendijk JJW, Raaymakers BW. Relative dosimetry in a 1.5 T magnetic field: an MR-linac compatible prototype scanning water phantom. Phys Med Biol 2014;59:4099–109.
[10] Raaymakers BW, Raaijmakers AJ, Lagendijk JJW. Feasibility of MRI guided proton therapy: magnetic field dose effects. Phys Med Biol 2008;53:5615–22.
[11] Fuchs H, Moser P, Gröschl M, Georg D. Magnetic field effects on particle beams and their implications for dose calculation in MR-guided particle therapy. Med Phys 2017;44:1149–56.
[12] Li JS. SU-E-J-201: investigation of MRI guided proton therapy. Med Phys 2015;42:3311.
[13] Moteabbed M, Schuemann J, Paganetti H. Dosimetric feasibility of real-time MRI-guided proton therapy. Med Phys 2014;41(111713):1–11.
[14] Hartman J, Kontaxis C, Bol GH, Frank SJ, Lagendijk JJW, van Vulpen M, et al. Dosimetric feasibility of intensity modulated proton therapy in a transverse magnetic field of 1.5 T. Phys Med Biol 2015;60:5955–69.
[15] Schellhammer SM, Gantz S, Lühr A, Oborn BM, Bussmann M, Hoffmann AL. Technical note: experimental verification of magnetic field-induced beam deflection and Bragg peak displacement for MR-integrated proton therapy. Med Phys 2018;45:3429–34.
[16] Schulz-Ertner D, Jäkel O, Schlegel W. Radiation therapy with charged particles. Semin Radiat Oncol 2006;16:249–59.
[17] Böhlen TT, Cerutti F, Dosanjh M, Ferrari A, Gudowska I, Mairani A, et al. Benchmarking nuclear models of FLUKA and GEANT4 for carbon ion therapy. Phys Med Biol 2010;55:5833–47.
[18] Parodi K, Mairani A, Brons S, Hasch BG, Sommerer F, Naumann J, et al. Monte Carlo simulations to support start-up and treatment planning of scanned proton and carbon ion therapy at a synchrotron-based facility. Phys Med Biol 2012;57:3759–84.
[19] Magro G, Dahle TJ, Molinelli S, Ciocca M, Fossati P, Ferrari A, et al. The FLUKA Monte Carlo code coupled with the NIRS approach for clinical dose calculations in carbon ion therapy. Phys Med Biol 2017;62:3814–27.
[20] Parodi K, Ferrari A, Sommerer F, Paganetti H. Clinical CT-based calculations of dose and positron emitter distributions in proton therapy using the FLUKA Monte Carlo code. Phys Med Biol 2007;52:3369–87.
[21] Ferrari A, Sala PR, Fasso A, Ranft J. FLUKA: a multi-particle transport code. Geneva: CERN; 2011.
[22] Simion P. Implementation of a solenoidal magnetic field map in FLUKA. FREIA Report Series; 2017. Last updated: 2017-04-25.
[23] Weber U, Kraft G. Design and construction of a ripple filter for a smoothed depth dose distribution in conformal particle therapy. Phys Med Biol 1999;44:2765–75.
[24] ICRP. 1990 Recommendations of the international commission on radiological protection. ICRP Publication; 1991.
[25] Ebner DK, Kamada T. The emerging role of carbon-ion radiotherapy. Front Oncol 2016;6:140.
[26] Jäkel O. The relative biological effectiveness of proton and ion beams. Z Med Phys 2008;18:276–85.
[27] Riboldi M, Orecchia R, Baroni G. Real-time tumour tracking in particle therapy: technological developments and future perspectives. Lancet Oncol 2012;13:e383–91.
[28] Oborn B, Dowdell S, Metcalfe PE, Crozier S, Mohan R, Keall PJ. Proton beam deflection in MRI fields: implications for MRI-guided proton therapy. Med Phys 2015;42:2113–24.